Bifurcations and traveling waves in a delayed partial differential equation

Alejandro D. Rey
Department of Chemical Engineering, McGill University, 3480 University Street, Montreal, Quebec H3A 2A7, Canada

Michael C. Mackey
Departments of Physiology, Physics, and Mathematics, and Centre for Nonlinear Dynamics in Physiology and Medicine, McGill University, 3655 Drummond Street, Montreal H3G 1Y6, Canada

(Received 18 November 1991; accepted for publication 1 April 1992)

Here cell population dynamics in which there is simultaneous proliferation and maturation is considered. The resulting mathematical model is a nonlinear first-order partial differential equation for the cell density $u(t,x)$ in which there is retardation in both temporal (t) and maturation variables (x), and contains three parameters. The solution behavior depends on the initial function $\varphi(x)$ and a three component parameter vector $P=(\delta,\lambda,r)$. For strictly positive initial functions, $\varphi(0)>0$, there are three homogeneous solutions of biological (i.e., non-negative) importance: a trivial solution $u_t\equiv 0$, a positive stationary solution u_{st}, and a time periodic solution $u_p(t)$. For $\varphi(0)=0$ there are a number of different solution types depending on P: the trivial solution u_t, a spatially inhomogeneous stationary solution $u_{nh}(x)$, a spatially homogeneous singular solution u_s, a traveling wave solution $u_{tw}(t,x)$, slow traveling waves $u_{stw}(t,x)$, and slow traveling chaotic waves $u_{scw}(t,x)$. The regions of parameter space in which these solutions exist and are locally stable are delineated and studied.

I. INTRODUCTION

A variety of mathematical models for biological dynamics are most appropriately framed as differential delay equations.[1] Many of these problems involve descriptions of cell replication, and in this circumstance the natural delay is the cell cycle time.

In this paper we consider a model for cell replication in which cells are both proliferating and maturing. The dynamical equation describing this situation is a novel first-order partial differential equation in which there is a retardation in the time variable as well as in the maturation variable. In Sec. II, we derive this equation, and in Sec. III we briefly discuss the numerical techniques we have employed in the investigation of the solution behavior. In Secs. IV and V we present the results of our investigation for initial functions drawn from two different classes. The paper concludes with a brief discussion in Sec. VI.

II. A MODEL FOR PROLIFERATING AND MATURING CELLULAR POPULATIONS

To put the model of this paper into a biological context, some brief introductory considerations may be helpful. Since the number of cell types is so varied, we illustrate these using the mammalian erythroid (red blood cell) production system.

Typically, cells have three types of generic behavior: they proliferate, they mature, and they die. With respect to proliferation, the cell cycle can be considered to be composed of four major phases: the initial resting or gap phases (G_0/G_1), followed by DNA synthesis, then another gap (G_2), to finally culminate in mitosis and cytokinesis (the production of two daughter cells). With respect to maturation, it is generally accepted that there is a population of pluripotential stem cells (PPSC) within the bone marrow that give rise to primitive stem cells committed to the production of erythrocytes, platelets, white blood cells, and lymphocytes. The committed (more mature) stem cells for the erythroid series (CSC-E) are assayed *in vitro* by the primitive and mature burst forming units (BFU-E) and colony forming units (CFU-E). These cells are then followed, with respect to maturity, by the erythroblasts. Throughout this hierarchy (but not including the PPSC) there is an increase in both the intracellular hemoglobin rate and content from the lowest in the BFU-E, through a maximal level in the most mature of erythroblasts. Finally, death is an event that can take place at any point within the cell cycle, as well as at different maturation levels.

Within the erythroid system there is a well-established local regulatory mechanism that exercises control over the proliferative rates within the BFU-E, CFU-E, and erythroblasts such that the proliferative rate (the rate that cells enter the cell cycle at the G_0/G_1 gap) is maximal at low cell numbers and monotonically decreases as cell numbers rise.

With these comments in mind, consider a population of cells that is capable of both proliferation and maturation. Actively proliferating cells are those actually in cycle that are committed to the replication of their DNA and the ultimate passage through mitosis and cytokinesis, with the eventual production of two daughter cells. The position of one of these cells within the cell cycle is denoted by a (cell *age*), which is assumed to range from $a=0$ (the point of commitment) to $a=\tau$ (the point of cytokinesis). In addition, each cell can be characterized by a maturation variable x whose range can be taken, without loss of generality, from $x=0$ to $x=1$. For concreteness one could think of the erythroid precursor cells and associate the maturation variable with the intracellular hemoglobin content. We as-

 1054-1500/92/020231-14$001.00

sume that cells die at a rate $\gamma \geqslant 0$, independent of age or maturation level, and mature (e.g., synthesize hemoglobin) with a velocity $V(x)$.

If we denote the density of proliferating cells by $U(t,x,a)$, then the conservation equation for $U(t,x,a)$ is given by

$$\frac{\partial U}{\partial t}+\frac{\partial U}{\partial a}+\frac{\partial [V(x)U]}{\partial x}=-\gamma U, \tag{1}$$

with the initial condition

$$U(0,x,a)=\Gamma(x,a), \qquad \text{for} \qquad (x,a)\in[0,1]\times[0,\tau]. \tag{2}$$

The total number u of proliferating cells of a given maturation level is defined in a natural way as

$$u(t,x)=\int_0^{\tau} U(t,x,a)da. \tag{3}$$

In completing the formulation of this problem, we specify the boundary condition

$$U(t,x,0)=2U(t,x,\tau)=\mathscr{F}(u(t,x)). \tag{4}$$

The first part of this boundary condition reflects the fact that the two daughter cells produced at the end of the cell division cycle form the input flux for the cell cycle. The second portion states that the input flux is a function $\mathscr{F}$ of the total number of cells at a given maturation level.[2]

To proceed beyond this point, for concreteness and to capture the observation that the hemoglobin synthesis rate increases as the hemoglobin content increases, we assume that the maturation velocity V has the form

$$V(x)=rx, \quad r>0. \tag{5}$$

Thus Eq. (1) becomes

$$\frac{\partial U}{\partial t}+\frac{\partial U}{\partial a}+rx\frac{\partial U}{\partial x}=-[\gamma+r]U, \tag{6}$$

with the same initial and boundary conditions stated before.

The general solution of Eq. (6) is

$$U(t,x,a)=\begin{cases}\Gamma(xe^{-rt},a-t)e^{-(\gamma+r)t}, & 0\leqslant t\leqslant a,\\ U(t-a,xe^{-ra},0)e^{(\gamma+r)a}, & a<t.\end{cases} \tag{7}$$

Integrating Eq. (6) over the age variable a gives

$$\frac{\partial u}{\partial t}+rx\frac{\partial u}{\partial x}=-[\gamma+r]u-\{U(t,x,\tau)-U(t,x,0)\}. \tag{8}$$

Utilizing the general solution (7) in conjunction with the boundary condition (4) gives

$$\frac{\partial u}{\partial t}+rx\frac{\partial u}{\partial x}=-[\gamma+r]u+\begin{cases}\Gamma(xe^{-rt},\tau-t)e^{-(\gamma+r)t}, & 0\leqslant t\leqslant\tau,\\ \mathscr{F}(u(t-\tau,xe^{-r\tau}))e^{(\gamma+r)\tau}, & \tau<t.\end{cases} \tag{9}$$

Equation (9) is the fundamental result of this section, and clearly demonstrates the time retardation $(t-\tau)$ as well as the spatial retardation $(xe^{-r\tau})$ that makes this particular model unique. When $r=0$, a variant of (9) describes the dynamic behavior observed in periodic hematopoiesis in both laboratory animals and humans.[2–4]

In this paper we focus on the solution properties of Eq. (9) when we take the proliferation rate to be $(1-u)$, a linearly decreasing function of u, as is observed biologically, so the input flux $\mathscr{F}$ at the start of the cell cycle is the product of this proliferation rate and the cell density u:

$$\mathscr{F}(u)=u(1-u),$$

set

$$\delta=\gamma+r, \quad \alpha=e^{-r\tau}, \qquad \text{and} \qquad \lambda=e^{(\gamma+r)\tau},$$

and pick $\tau=1$ without loss of generality, so (9) is equivalent to

$$\frac{\partial u}{\partial t}+rx\frac{\partial u}{\partial x}=-\delta u+\lambda u_{\tau}(1-u_{\tau}), \tag{10}$$

where $u_{\tau}\equiv u(t-1,xe^{-r})$. To complete the specification of the problem requires an initial condition, and we use the special one:

$$u(t-1,xe^{-r})\equiv\varphi(x), \qquad \text{for} \qquad (t,x)\in[0,1]\times[0,1]. \tag{11}$$

In the remainder of this paper we study the solutions of (10) to obtain insight into the modes of dynamic behavior that are possible and their dependence on the initial function φ, which would correspond to the cell numbers entering from the PPSC compartment. A number of authors[5–11] have studied the global stability properties of a class of partial differential equations that includes Eq. (9) when $\tau=0$. These results indicate that when $\varphi(0)>0$ the solutions of (9) (with $\tau=0$) will be globally asymptotically stable. However, when $\varphi(0)=0$ the solutions are chaotic on a function space. To our knowledge there are no analytic results to give insight into solution behavior when $\tau>0$, and this is of potential interest, since both chemotherapy and radiotherapy are capable of reducing the PPSC input to zero, corresponding to $\varphi(0)=0$.

As shown below, the characteristics $x(t)$ of Eq. (2) are strictly non-negative for all times t, and no boundary condition is required, except for the case $\varphi(0)=0$, in which case we impose the condition $u(t,x=0)=0$.

III. NUMERICAL METHODS

Equation (10) is studied for two cases: (i) $\varphi(0)>0$ and (ii) $\varphi(0)=0$. Due to the complex behavior encountered in the study of this problem, we used two numerical approaches.

A. Galerkin finite elements method

In the absence of large spatial gradients, $\partial u/\partial x \simeq \mathscr{O}(1)$, we use the Galerkin finite elements method (GFEM[12]) for spatial discretization, with a first-order implicit corrector–predictor time integration scheme.

Briefly, given a partial nonlinear differential equation $L(u)=0$ in a domain D, with the appropriate initial and boundary conditions in D, the method assumes that u is accurately represented by an approximate solution u_a:

$$u_a(t,x)=\sum_{j=1}^{N} u_j(t)\phi_j(x), \tag{12}$$

where the ϕ_j are known basis functions, the u_j are the unknown coefficients, and N is the number of nodes in the spatial discretization. Since the basis functions are chosen to be equal to unity at the nodes, the unknown coefficients u_j are equal to the approximate solution u_a at the nodes. Substitution of (12) into the equation $L(u)=0$, gives the nonzero residual R:

$$R=L(u_a)=\sum_{j=1}^{N} u_j\phi_j. \tag{13}$$

To obtain the unknown coefficients the residual R is forced to zero in the following integral sense:

$$F_k=(R,\phi_k)=\int_D R\phi_k\,dx=0, \quad k=1,\ldots,N, \tag{14}$$

where the ϕ_k are the weighting functions. In the Galerkin method the weighting functions are equal to the basis functions. If L is a nonlinear differential operator the spatial discretization leads to a set of nonlinear ordinary differential equations $F_k=0, k=1,\ldots,N$, which can be solved by the Newton–Raphson method or any other root finder.

In this work we use the linear basis and weighting functions. The spatial domain consists of 30–500 elements. A uniform node distribution is used, except for the cases where a boundary layer and wave trains develop. The time integration scheme is a first-order implicit predictor–corrector method (forward Euler–backward Euler) with a fixed time step $h=10^{-2}$. The resulting implicit set of nonlinear algebraic equations for the unknown coefficients u_j are solved using the Newton–Raphson iteration scheme.

B. Integration along characteristics

In the presence of large spatial gradients $[\partial u/\partial x \gg \mathcal{O}(1)]$, spatial discretization is inadequate and time integration along the characteristics of Eq. (2) may be employed.

Along the x characteristics, $x(t)=\xi e^{rt}$, Eq. (2) can be rewritten as

$$\frac{du}{dt}=-\delta u+\lambda u_\tau(1-u_\tau), \tag{15}$$

where

$$u(t,x(t))\equiv u(t,\xi e^{rt}) \tag{16a}$$

and

$$u_\tau(t,x(t))\equiv u(t-1,\xi e^{r(t-1)}); \tag{16b}$$

ξ is a parameter that defines each characteristic $[x(t=0)=\xi]$, and d/dt denotes the total derivative (time derivative) along the characteristics:

$$\frac{du(t,x)}{dt}\equiv\frac{\partial u(t,x)}{\partial t}+rx(t)\frac{\partial u}{\partial x(t)}. \tag{17}$$

In the rest of this paper we use the convention that $x(t)=\xi e^{rt}$ denotes the value of the maturation at a given time t on a given characteristic defined by ξ, which denotes a fixed maturation value. From Eq. (16) it follows that integration along the characteristics eliminates the need to perform any spatial interpolation due to the spatial retardation e^{-r}, and thus dispenses with errors associated with the spatial discretization. We use an Euler explicit corrector–predictor again with a constant time step of $h=10^{-2}$:

$$u_{pr}(t+h,\xi e^{r(t+h)})=u(t,\xi e^{rt})+hf(u(t,\xi e^{rt})), \tag{18a}$$

$$u_c(t+h,\xi e^{r(t+h)})=u(t,\xi e^{rt})+hf(u_{pr}(t+h,\xi e^{r(t+h)})), \tag{18b}$$

$$f(u(t,\xi e^{rt}))=-\delta u(t,\xi e^{rt})+\lambda u(t-1,\xi e^{r(t-1)})\times[1-u(t-1,\xi e^{r(t-1)})]. \tag{18c}$$

Higher-order schemes are easy to implement, but the accuracy of the method, established from comparison with known analytical solutions of Eq. (10) for no delay and bifurcation results (see Sec. III below), is more than satisfactory.

IV. RESULTS FOR $\varphi(0)>0$

A. Local analysis

Extensive numerical simulation indicates that representative solution behavior is obtained with $\varphi(x)=x+c$ for $c>0$.

For $0<\lambda<\delta$ it is clear that the only non-negative (and therefore biologically meaningful) stationary spatially homogeneous solution to Eq. (15) is the trivial solution $u_t\equiv 0$. For $\lambda>\delta$ there is a second solution given by $u_{st}=(\lambda-\delta)/\delta$ that coexists with u_t.

1. Stability of the trivial solution

To examine the local stability of the trivial solution we linearize (15) about u_t to give

$$\frac{dz}{dt}=-\delta z+\lambda z_\tau, \tag{19}$$

wherein $z=u-u_t$. The associated eigenvalue is given implicitly by

$$\mu=-\delta+\lambda e^{-\mu\tau}, \tag{20}$$

and it is a straightforward matter to show that $\mu<0$ for $0<\lambda<\delta$, $\mu\equiv 0$ for $\lambda=\delta$, and $\mu>0$ for $\lambda>\delta$. Thus when the trivial solution u_t is the only non-negative homogeneous solution it is locally stable, and loses its stability as soon as the second homogeneous solution u_{st} exists.

2. Stability of the homogeneous solution

Next we examine the stability of u_{st}. Again linearizing Eq. (15) gives

$$\frac{dz}{dt} = -\delta z + (2\delta - \lambda) z_\tau, \tag{21}$$

where $z = u - u_{st}$. Now, assuming a time periodic solution of the form $e^{(\mu + i\omega)t}$, we obtain

$$\mu + i\omega = -\delta + (2\delta - \lambda) e^{-\mu} e^{i\omega}. \tag{22}$$

Separating (22) into real and imaginary parts gives

$$\mu = -\delta + (2\delta - \lambda) e^{-\mu} \cos \omega, \tag{23a}$$

$$\omega = (2\delta - \lambda) e^{\mu} \sin \omega. \tag{23b}$$

For (δ,λ) such that

$$\sqrt{(2\delta - \lambda)^2 - \delta^2} < \cos^{-1}\left(\frac{\delta}{2\delta - \lambda}\right), \tag{24}$$

using the criteria of Hayes[13] it is easy to show that $\mu < 0$, and when the inequality is reversed, $\mu > 0$. Thus, whenever (24) is satisfied we know that u_{st} is locally stable.

3. Bifurcation to a periodic solution

It is straightforward to show that $\mu \equiv 0$ when (δ,λ) satisfy

$$\sqrt{(2\delta - \lambda)^2 - \delta^2} = \cos^{-1}\left(\frac{\delta}{2\delta - \lambda}\right). \tag{25}$$

We denote the unique solution of (25) by $\lambda^b(\delta)$. This condition corresponds to a periodic solution u_p of the linear equation (21) with period

$$T = \frac{2\pi}{\omega} = \frac{2\pi}{\sqrt{(2\delta - \lambda)^2 - \delta^2}}. \tag{26}$$

The limiting conditions of Eqs. (23) and (25) are as $\delta \to 0$, $\omega \to \pi/2$, and as $\delta \to \lambda, \omega \to \pi$. The period T of the temporal oscillation satisfies $2 \leqslant T \leqslant 4$.

Thus, when (25) is satisfied so $\lambda \equiv \lambda^b(\delta)$, there is a Hopf bifurcation[14] from the spatially homogeneous stationary solutions u_{st} to a periodic solution u_p of period T along the characteristics $x(t) = \xi e^{rt}$. Close to the Hopf bifurcation, after the initial transients die out, the periodic solutions $u_p(t,x(t))$ along the characteristics, are approximately given by

$$u_p(t,x(t)) \simeq \frac{\lambda - \delta}{\lambda} + \epsilon \cos(\omega t); \quad \epsilon \ll 1, \quad 0 \leqslant x \leqslant 1. \tag{27}$$

Note that this implies that

$$u_p(t,\xi e^{rt}) = u_p(t + T, \xi e^{r(t+T)}). \tag{28}$$

Equation (28) also shows that the solution behavior is determined solely from the characteristics in the immediate vicinity of $x = 0$, that is as $\xi \to 0$. Since in this section we are studying the long time solution behavior for $\varphi(x) = x + c$ with $c > 0$, it is clear that the initial information is determined solely by c. Given $c > 0$, no matter how small, for sufficient long times the solution behavior in the entire maturation domain $0 < x \leqslant 1$ is determined by the characteristics emanating from near the origin and carrying the same information $\varphi(0) = c$.

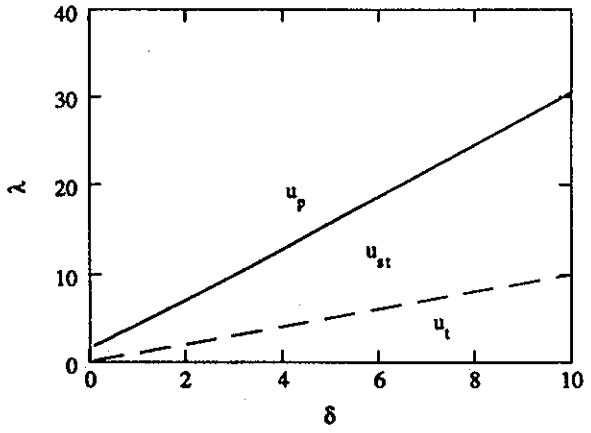

FIG. 1. Bifurcation diagram in the (δ,λ) plane, for Eq. (10) with $\varphi(0) > 0$. The Hopf bifurcation curve (full line) was obtained from Eq. (24) and from numerical integration of Eq. (10). Above the bifurcation curve the solutions are spatially homogeneous and time periodic. Within the region bounded above by the bifurcation line and below by the line $\lambda = \delta$, the solutions are stationary and spatially homogeneous: $u_s = (\lambda - \delta)/\lambda$. For $\lambda \leqslant \delta$ the stable stationary solution is the trivial solution $u_t = 0$.

The time scale of this transfer is set by the parameter r and $\varphi(0) = c > 0$. The characteristic time required to carry the initial information from a location $x(t = 0) = \epsilon \ll \varphi(0)$ to $x = e^{-1}$ is $t^* = r^{-1}$. Thus, for large r the characteristic time t^* vanishes and the resulting periodic solutions u_p set in at once, while as $r \to 0$ the characteristic time diverges and a transient pattern lasts for an infinitely long time.

To summarize: (1) for every pair $(\delta,\lambda) = (\delta,\lambda^b(\delta))$ obtained from (25) there is a Hopf bifurcation along the characteristics; (2) at sufficiently long times the solution behavior is set solely by the information emanating from the characteristics next to the origin $(t,x) = (0,0)$; and (3) the time scale of the pattern for a given $\varphi(0)$ is set by the magnitude of r. Our numerical results (see below) confirm these three observations.

Figure 1 shows the bifurcation diagram in the (λ,δ) plane, obtained from Eqs. (20) and (25) for the case of $\varphi(0) > 0$. The full line denotes the temporal Hopf bifurcation on which there are periodic solutions and below which the solutions are spatially homogeneous and stationary. These spatially homogeneous solutions are of two types. Below the $\lambda = \delta$ line they are the trivial solutions u_t, and for $\delta < \lambda < \lambda^b$ they are the positive solutions u_{st}. It will be shown in the next section that numerically the periodic solutions are spatially homogeneous, as expected from the analysis.

B. Numerical results

In this section we use an initial function $\varphi(x) = x + 0.1$.

Figure 2 shows the evolution of $u(t,x(t))$ along three characteristics for parameters just above the Hopf bifurcation line, demonstrating that along the characteristics the solutions oscillate around the spatially homogeneous steady state u_{st} with constant amplitude. The calculated period obtained from Eq. (25) is $T = 3.09$, consistent with

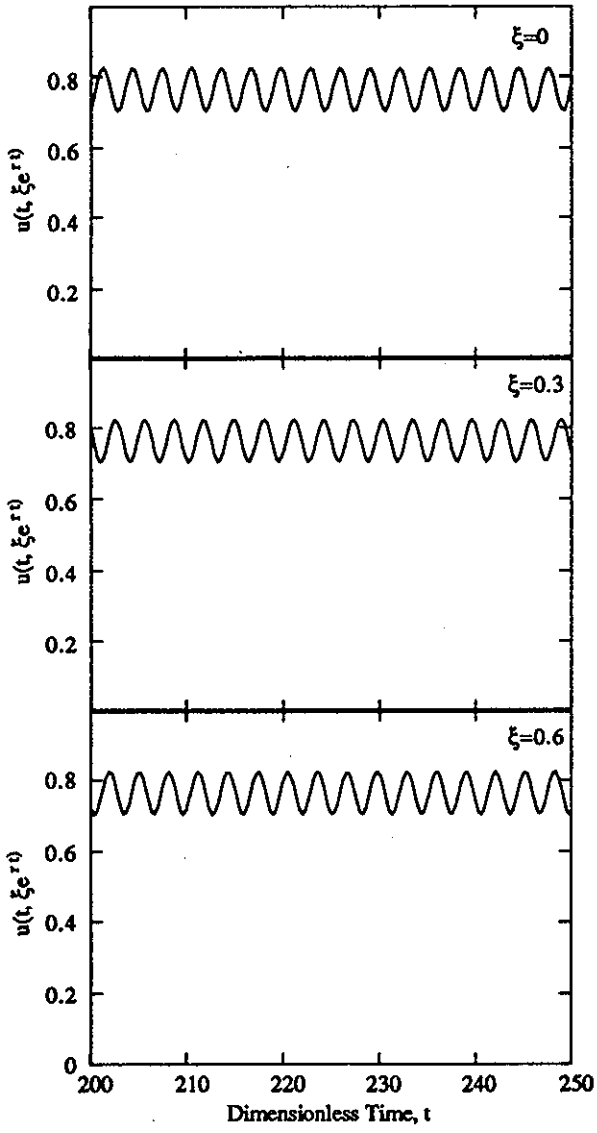

FIG. 2. Evolution of cell populations $u(t,xe^{rt})$ along three characteristics: $\xi = 0$, 0.3, and 0.6; $(\delta,\lambda,r) = (1,4.3,0.0001)$. After initial transients die out the solutions are periodic along the characteristics: $u(t + T,xe^{r(t+T)})$, and oscillate with constant amplitude around the homogeneous stationary solutions $u_s = (\delta - \lambda)/\lambda = 0.7674$, with a period of $T = 3.1$.

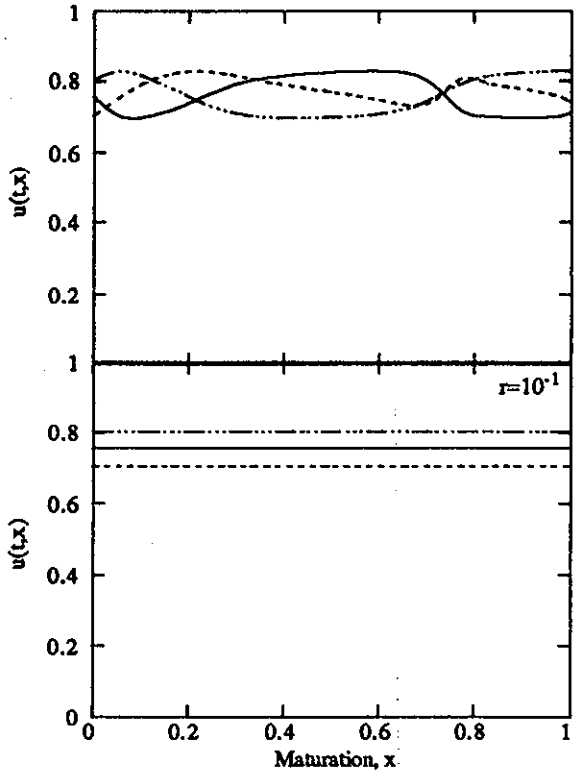

FIG. 3. Effect of r on the evolving spatial distribution of cell populations $u(t,x)$. $(\delta,\lambda) = (1,4.3)$. Top $r = 0.001$, bottom $r = 0.1$. $t = 100.2$ (full), 101.1 (dash), 102 (dash–triple dotted). The time scale to have spatially homogeneous periodic solutions is $t^* = r^{-1}$, $\epsilon \ll 1$ $\varphi(0) = 0.1$. For $r = 0.001$ the solutions are spatially inhomogeneous since they are given by superposition of out-of-plane oscillations. For $r = 0.1$ the solutions are homogeneous, since they are the result superposition of in-phase oscillations.

the period of the oscillations shown in Fig. 2. Higher-order bifurcations are likely to be present at larger values of λ than those considered here, but they are beyond the scope of this paper.

Next we address the question of time scales and the nature of the evolving solutions in the (t,x) space close to the Hopf bifurcation. Figure 3 shows $u(t,x)$ as a function of maturation at three consecutive times for two values of r. For small r the profiles are inhomogeneous, oscillating around the steady-state values with amplitudes as shown in Fig. 2. For small r (long time scales) the solution $u(t,x)$ results from a linear superposition of waves of equal amplitude but different time varying phase, and hence the profiles are not periodic, $u(t,x) \neq u(t + T,x)$, at fixed x. For larger r the time scale t^* is smaller and the solution for a given time is homogeneous since, for all x, the information is coming from the characteristics next to the origin $(t,x) = (0,0)$ and hence from the same constant value $\varphi(0) = 0.1$. Since r defines the time scale t^* of evolution toward a spatially homogeneous time periodic solution, we conclude that at any given time the solutions are either spatially inhomogeneous transient solutions $(t^* > t)$ or spatially homogeneous time periodic solutions $(t^* < t)$ according to the magnitude of r.

We next show that for relatively small r the transient inhomogeneous solutions evolve, at sufficiently long times, into spatially homogeneous periodic solutions. Figure 4 shows the evolving $u(t,x)$ profiles for small r and three sets of times $t = 100.2 + nT$, $101.1 + nT$, $102 + nT$. The top figure $(n = 0)$ shows a typical transient inhomogeneous profile constrained in a band defined by the amplitude of the oscillations along the characteristics. The middle figure $(n = 100)$ shows the profiles are being stretched, but continue to be confined in the same band. The stretching effect is a result of time periodicity along the characteristics, $u(t,x(t)) = \mu(t + nT,x(t + nT))$, demonstrating that after n cycles the value of u at a given x will be the same value that it had at $x(t - nT)$. After sufficiently many cycles the profiles are stretched, and eventually approach spatially homogeneous cell populations, since at a given time all values of u are the result of the same initial data coming

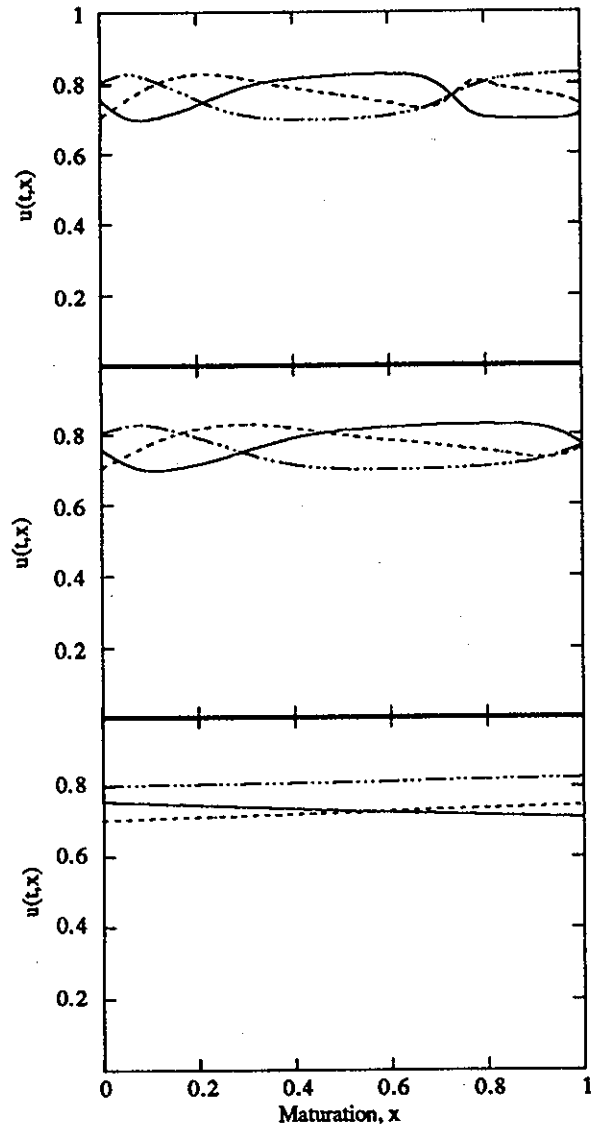

FIG. 4. Evolution of inhomogeneous cell populations $u(t,x)$ for $r \ll 1$. $P = (\delta,\lambda,r) = (1,4.3,0.001)$. $t = 100.2 + nT$ (full), $101.1 + nT$ (dash), $102 + nT$ (dash–triple dotted). Top $n = 0$, middle $n = 100$, bottom $n = 1000$. For $r \ll 1$ there is a low speed of transmission of the initial data close to the origin $(t,x) = (0,0)$ into the whole maturation range $0 < x \leqslant 1$. At sufficiently long times $t > t^*$ the profiles stretch out and eventually become homogeneous.

from the characteristics next to the origin $(t,x) = (0,0)$. This is shown in the lower figure ($n = 1000$) in which u is almost totally homogeneous and time periodic.

Summary: The main conclusions of this section, summarized in Table I, are as follows.

(1)If $\varphi(0) > 0$ the stationary spatially homogeneous solutions $u_{st} = (\lambda - \delta)/\delta$ to Eq. (10) undergo a Hopf bifurcation at a given value of $(\delta,\lambda) = (\delta,\lambda^b(\delta))$ given by Eq. (25). The resulting solutions are periodic along the characteristics of Eq. (10).

(2) The eventual solution behavior depends on the value of the initial function near the origin $\varphi(\epsilon)$ with $\epsilon \ll 1$. For the choice $\varphi(x) = 0.1 + x$, at sufficiently long times all the characteristics ξe^{rt} crossing the maturation interval $0 \leqslant x \leqslant 1$ carry the same information from the initial data

TABLE I. $\phi(0) > 0$ (Secs. IV A and IV B).

Parameters	Solution type	Symbol	Figure number
$0 < \lambda \leqslant \delta$	trivial	u_t	1
$\delta < \lambda < \lambda^b$	stationary, spatially homogeneous	u_{st}	1,2
$\lambda^b \leqslant \lambda$	time periodic spatially homogeneous	u_p	1,3,4

$\varphi(0)$, and hence the solutions are eventually spatially homogeneous and time periodic.

(3) For a given $\varphi(0) > 0$, the time required to achieve the homogeneous time periodic behavior depends on the magnitude of r that sets the speed of transmission of information from the region next to the origin $(t,x) = (0,0)$ to the entire maturation range $0 \leqslant x \leqslant 1$.

V. RESULTS FOR $\varphi(0) = 0$

A. Local analysis

In this section we present the local analysis of Eq. (10) when the initial function vanishes for zero maturation, $\varphi(0) = 0$. We use the numerical techniques described briefly in Sec. II. Before presenting and discussing the numerical results we present some analytical results that are crucial in constructing the bifurcation diagram.

1. Background

As discussed in Rey and Mackey[15] when $\varphi(0) = 0$ and $0 < \lambda < \delta$, the single stationary solution to (10) is the trivial solution $u_t \equiv 0$. However, when $0 < \delta < \lambda$, the stationary solutions to Eqs. (10) are chaotic in a function space, and there is no longer a unique globally asymptotically stable steady state. Rather, there are three families of stationary solutions: a trivial solution $u_t = 0$, a spatially nonuniform solution $u_{nh}(x)$, and a singular solution,

$$u_s(x) = \begin{cases} \dfrac{\lambda - \delta}{\lambda}, & x > 0, \\ 0, & x = 0, \end{cases} \tag{29}$$

according to the values of the parameter vector $P = (\delta,\lambda,r)$. Furthermore, for a given P the spatially inhomogeneous solution is not unique and depends on the initial function $\varphi(x)$.

In this paper we restrict our study to $\varphi(x) = x$. In Rey and Mackey[15] we showed numerically that for $\varphi(x) = x$ there were three possible stationary stable solutions to Eq. (10) depending on the value of r relative to a critical value r_c: (1) for $r < r_c$, the singular solution $u_s(x)$; (2) for $r = r_c$ there is an inhomogeneous solution $u_{nh}(x)$ for $x \geqslant 0$; and (3) for $r > r_c$ there is a trivial solution $u_t \equiv 0$ for $x \geqslant 0$.

The parameter vector P at which there is a loss of stability of the trivial solution u_t with $\varphi(x) = x$ is found from linearizing Eq. (15) around the trivial solution:

$$\frac{dz}{dt} = -\delta z + \lambda z_\tau, \tag{30}$$

where z represents infinitesimal perturbations to the trivial solution along the characteristics, so

$$z(t,x(t)) = z(t,\xi e^{rt})$$

and

$$z_\tau(t,x(t)) = z(t-1,\xi e^{r(t-1)}).$$

For perturbations of the form $z(t,\xi e^{rt}) = \epsilon \xi e^{rt}$ with $\epsilon \ll 1$, we find

$$r = -\delta + \lambda e^{-r}, \tag{31}$$

establishing that a spatially inhomogeneous solution is marginally stable if $r \equiv r_c$, where r_c is the unique solution of (31). For $0 < r < r_c$, the trivial solution is unstable to infinitesimal spatially linear perturbations, but stable to those perturbations if $r > r_c$.

These local stability results, valid for linear spatial perturbations, have been studied numerically by integration of Eqs. (10) and (15) for $\varphi(x) = x$, $0 < \delta \leqslant 10$, and $10^{-6} \leqslant r \leqslant 1.1$. For any given value of (δ,λ) we always found that there is a critical $r = r_c$, given by Eq. (31), for which the stationary solution is the spatially inhomogeneous solution $u_{\rm nh}$; if $r < r_c$ the stationary solution is the singular solution, and if $r > r_c$ it is the trivial solution.

Denote the value of P satisfying Eq. (31) by P^s and define

$$\lambda^s \equiv \lambda^s(\delta,r) = (\delta + r)e^r \tag{32}$$

as the curve in the (δ,λ) plane on which $u_{\rm nh}$ is the stable solution for the given value of r. We note that by increasing r, λ^s increases for a given δ. In Rey and Mackey,[15] using Galerkin finite elements with 30 linear basis functions we found that for $(\delta,\lambda) = (2,4)$, $r_c \simeq 0.469\,31$, while Eq. (31) predicts $r_c \simeq 0.4785$, an error of 1.9%. This accuracy is greatly improved by integrating along the characteristics since we dispense with errors incurred by spatial discretization.

In Rey and Mackey[15] we also showed that when r is close to r_c the cell population evolves toward the trivial or the singular solution very slowly, in analogy to the critical slowing down observed in phase transitions. Furthermore, we showed that when r is less than r_c the solution slowly evolves with the formation of a boundary layer in the immediate vicinity of $x = 0$. We then expect that for a given (δ,r) if λ is close to but larger than λ^s the solution will exhibit the slowing down and boundary layer behavior described above, evolving on a time scale proportional to $\lambda - \lambda^s$. Therefore if spatial oscillations are present, they will be transported with a velocity dictated by the dynamics of the boundary layer.

2. Bifurcations of the singular solution to a traveling wave

We now address the possible existence of a Hopf bifurcation of the singular solution u_s into a traveling wave solution $u_{\rm tw}(t,x)$ when λ becomes sufficiently large. Linearizing Eq. (10), for $x > 0$, around the singular solution u_s:

$$u(t,x) = u_s(x) + z(t,x),$$

we obtain

$$\frac{\partial z}{\partial t} + rx\frac{\partial z}{\partial x} = -\delta z + (2\delta - \lambda)z_\tau, \tag{33}$$

where $z_\tau = u(t-1,xe^{-r})$. Introducing the change of variables $x = e^y$ gives

$$\frac{\partial z}{\partial t} + r\frac{\partial z}{\partial y} = -\delta z + (2\delta - \lambda)z_\tau, \tag{34}$$

with $z_\tau = u(t-1,y-r)$. Motivated by numerical simulations we seek solutions of the form

$$z(t,x) = e^{i\omega(1-r)t}e^{i\omega y}. \tag{35}$$

Substituting (35) into (34) gives the same relations (23) to (26) that we obtained in our investigation of the spatially homogeneous solution $u_{\rm st}$ in Sec. IV. Again, for a given δ the value of λ that satisfies Eq. (24) is denoted by λ^b. This means that for $0 < r < 1$, values of $(\delta,\lambda = \lambda^b > \lambda^s)$ that satisfy Eq. (24) will result in a simultaneous temporal and spatial Hopf bifurcation of u_s and give rise to left traveling waves. We therefore expect that for $r < 1$ and with a λ infinitesimally larger than λ^b the solutions to Eq. (10), after transients die out, will be approximately given by

$$u_{\rm tw}(t,x) \simeq \begin{cases} \dfrac{\lambda - \delta}{\lambda} - \epsilon\cos(\omega((1-r)t + \ln x)), & x > 0, \\ 0, & x = 0, \end{cases} \tag{36}$$

with $\epsilon \ll 1$. Alternately, along the characteristics $(\xi > 0)$ they are

$$u_{\rm tw}(t,\xi e^{rt}) \simeq \begin{cases} \dfrac{\lambda - \delta}{\lambda} - \epsilon\cos(\omega(t + \ln \xi)), & x > 0, \\ 0, & x = 0. \end{cases} \tag{37}$$

In the (t,x) plane these solutions are left traveling waves, with an angular frequency $\omega^* = \omega(1-r)$ and a constant wave vector $k = \omega$ in a logarithmic scale that diverges as $x \to 0$ in a linear maturation scale. The hyperbolic waves are not dispersive since in a logarithmic maturation scale the phase velocity $U = \omega^*/k$ is equal to the group velocity $G = d\omega^*/dk$:

$$U = G = (1-r). \tag{38}$$

The wave propagates to the left with a velocity in a linear maturation scale vanishes at $x = 0$. On a logarithmic maturation scale the constant wavelength L of the traveling pattern is given by $L = e^{T_c}$, where $T_c = 2\pi/\omega$ is the period of the temporal oscillation observed along the characteristics, and L is constrained by $e^2 \leqslant L \leqslant e^4$. Note that the wavelength L (the ratio of the locations of two successive

TABLE II. $\phi(0) = 0$ (Secs. V A and V B).

Parameters			Solution type	Symbol	Figure number
$0 < r \leqslant r_{\min}$	$0 < \delta \leqslant \delta_{\max}$	$0 < \lambda < \lambda^s$	trivial	u_t	5,8
		$\lambda = \lambda^s$	stationary, spatially inhomogeneous	u_{nh}	5,8
		$\lambda^s < \lambda < \lambda^b$	singular, stationary, spatially homogeneous	u_s	5,8 9,10
		$\lambda^b \leqslant \lambda$	traveling waves	u_{tw}	5,6 7,9
$r_{\min} < r < r_{\max}$	$0 < \delta < \delta^* \leqslant \delta_{\max}$	$\lambda < \lambda^s$	trivial	u_t	5,13
		$\lambda = \lambda^s$	stationary, spatially inhomogeneous	u_{nh}	5,13
		$\lambda^s < \lambda$	slow traveling waves	u_{stw}	5,11,12,13
	$0 < \delta^* < \delta \leqslant \delta_{\max}$	$0 < \lambda < \lambda^s$	trivial	u_t	5
		$\lambda = \lambda^s$	stationary, spatially inhomogeneous	u_{nh}	5
		$\lambda^s < \lambda < \lambda^b$	singular, stationary spatially homogeneous	u_s	5
		$\lambda^b \leqslant \lambda$	slow traveling waves	u_{stw}	5,11,12
$r_{\max} \leqslant r$	$0 < \delta \leqslant \delta_{\max}$	$\lambda < \lambda^s$	trivial	u_t	5
		$\lambda = \lambda^s$	stationary, spatially inhomogeneous	u_{nh}	5
		$\lambda^s \leqslant \lambda$	slow chaotic traveling waves	u_{scw}	5 15,16,17

troughs) is independent of r, but depends on (δ,λ). Furthermore, the period along the characteristics is related to the period T_x in the (t,x) plane by

$$T_x = \frac{T_c}{1 - r}. \tag{39}$$

It will be shown in the next section that the apparent divergence at $r = 1$ never occurs since other dynamics set in this region of the parameter space.

3. Bifurcation of the inhomogeneous solution u_{nh}

We next examine in more detail the situation in parameter space in which the line corresponding to the spatially inhomogeneous solution $u_{\text{nh}}(x)$ intersects the Hopf bifurcation line λ^b. Substituting $\lambda = (\delta + r)e^r$ into Eq. (25) gives

$$\frac{\delta}{2\delta - (\delta + r)e^r} = \cos\sqrt{[2\delta - (\delta + r)e^r]^2 - \delta^2}, \tag{40}$$

which for $\delta = 0$ gives $r_{\min} \simeq 0.7455$. The maximum value of r for the intersection of the curves λ^s and λ^b is also found from Eq. (40) by noting that in the limit $\lambda^s = \lambda^s(\delta \to \infty, r)$ and $\lambda^b = \lambda^b(\delta \to \infty)$,

$$\frac{\delta}{2\delta - (\delta + r)e^r} = \frac{1}{2 - e^r}, \tag{41}$$

and that $\omega \to \pi$, which yields $r_{\max} \equiv \ln 3 \simeq 1.0986$. Thus Eq. (40) defines a value of $\delta = \delta^*$ for which $\lambda^s = \lambda^b$.

Collecting the above observations we conclude (see Table II) the following.

(1) When $r \leqslant r_{\min}$ and $\lambda > \lambda^b > \lambda^s$ the solution consists of left traveling waves with a velocity (wave vector) that vanishes (diverges) as $x \to 0$.

(2) When $r_{\min} < r \leqslant r_{\max}$ and $\lambda > \lambda^s > \lambda^b$ or $\lambda > \lambda^b > \lambda^s$ the solution consists of slow left traveling waves with a diverging wave vector, but with a propagation speed set by the controlling slow dynamics of the boundary layer.

(3) When $r_{\max} < r$ then $\lambda^s > \lambda^b$ for any δ. If $\lambda > \lambda^s$ it will be shown in the next section that the solution slowly evolves to a transient chaotic state described by slow left traveling waves $u_{\text{scw}}(t,x)$ of a diverging wave vector, but with oscillations around time and space varying cell densities.

Each of these situations is associated with a distinct bifurcation diagram in the (δ,λ) plane for $\varphi(x) = x$, as shown in Fig. 5.

(1) For $r = r_{\min}$, $\lambda^b = \lambda^s$ at $\delta = 0$, and the bifurcation diagram consists of three regions (three stable stationary solutions and a traveling wave solution) defined by λ^s and λ^b, with $\lambda^b > \lambda^s$ when $\delta > 0$. For $\lambda \geqslant \lambda^b$ the stable solution is u_{tw}, when $\lambda^s < \lambda < \lambda^b$ the stable solutions are the stationary spatially homogeneous singular solutions u_s, when $\lambda < \lambda^s$ the stable solutions are trivial solutions, u_t, and when $\lambda = \lambda^s$ the stable solutions are the stationary spatially inhomogeneous solutions u_{nh}. This also represents all $r < r_{\min}$ cases, since the bifurcation line always lies above the stability line.

(2) For $r_{\min} < r = 1 < r_{\max}$, $\lambda^b = \lambda^s$ at $0 < \delta = \delta^*$, and the bifurcation diagram consists of three regions (three stable stationary solutions and a slow traveling wave solution) defined by λ^s and λ^b, with $\lambda^b > \lambda^s$ when $\delta > \delta^*$. For $\lambda \geqslant \lambda^s > \lambda^b$ and $\delta \leqslant \delta^*$ the stable solution is u_{stw}, but when $\lambda^s < \lambda < \lambda^b$ and $\delta > \delta^*$ the stable solutions are the stationary spatially homogeneous singular solutions u_s, when $\lambda < \lambda^s$ the stable solutions are trivial solutions, u_t, and when $\lambda = \lambda^s$ the stable solutions are the stationary spatially inhomogeneous solutions u_{nh}.

(3) For $r > r_{\max}$, $\lambda^b < \lambda^s$ for all δ, and the bifurcation diagram consists of two regions (three stable stationary solutions) defined by λ^s. If $\lambda > \lambda^s$ the stable solutions are slow chaotic traveling waves u_{scw}, if $\lambda = \lambda^s$ the stable solutions are the stationary spatially inhomogeneous solutions u_{nh}, and if $\lambda < \lambda^s$ the stable solutions are the trivial solutions u_t.

In the following section we provide numerical evidence for these points.

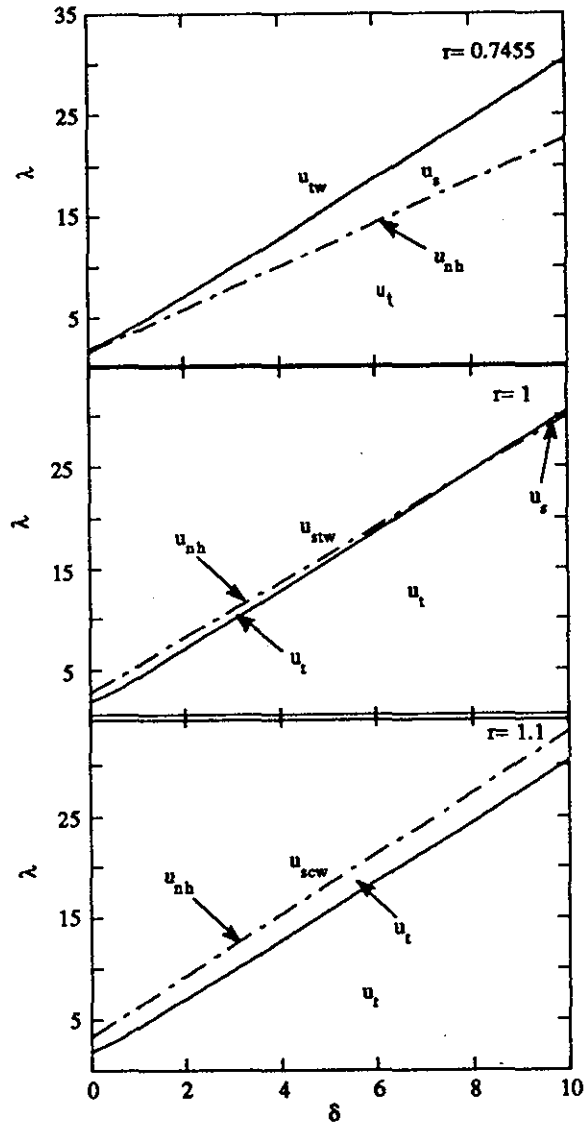

FIG. 5. bifurcation diagram corresponding to Eq. (10), with $\varphi(x) = x$, in the (δ,λ) plane for three representative values of $r \geqslant r_{\min} = 0.7455$: $r = r_{\min}$ (top), $r = 1$ (middle), and $r = 1.1 > r_{\max} = \ln 3$ (bottom). The full line represents the Hopf bifurcation line and the dashed line represents the stationary inhomogeneous solutions. For $0.7455 < r < \ln 3$ the two lines intersect. Proximity to the dashed line always involves very slow dynamics. The six possible solutions are the trivial solution u_t, the spatially inhomogeneous stationary solution u_{nh}, the singular solution u_s, hyperbolic traveling waves u_{tw}, slow traveling waves u_{stw}, and slow chaotic waves u_{scw}.

B. Numerical solutions

4. $0 < r \leqslant r_{min}$

Figure 6 shows the evolution of the cell density along three characteristics for $\lambda^s < \lambda^b < \lambda$. The solution oscillates with an eventually constant amplitude around u_s. Figure 6 shows that the solutions are in phase since the characteristics were chosen such that $\xi_3 = \xi_2 e^{T_c} = \xi_1 e^{2T_c}$. The period $T_c = 2.36$ is in accordance with the period calculated from Eq. (26).

Figure 7 shows the evolution of the cell density in the $(t,\ln x)$ plane for the same parameters and three different times obtained using GFEM. The time intervals of 4.8 are

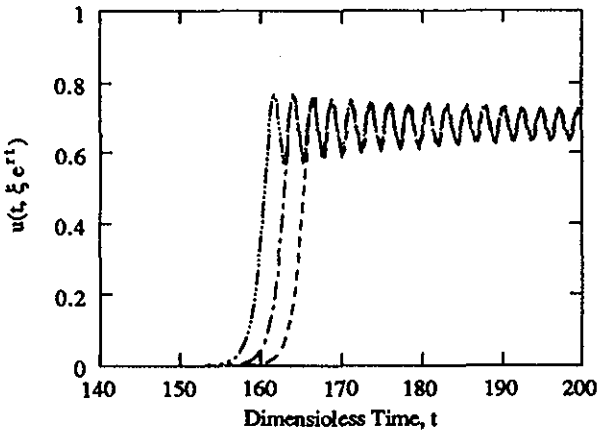

FIG. 6. Cell density evolution along three characteristics: $(\xi_1,\xi_2,\xi_3) = (0.2\times10^{-70},2.118\times10^{-70},22.43\times10^{-70})$ for $(\delta,\lambda,r) = (5,15.7,0.5)$. $\lambda^b = 15.661$, $\lambda^s = 9.067$, $T_c = 2.367$, and $u_s = 0.681$.

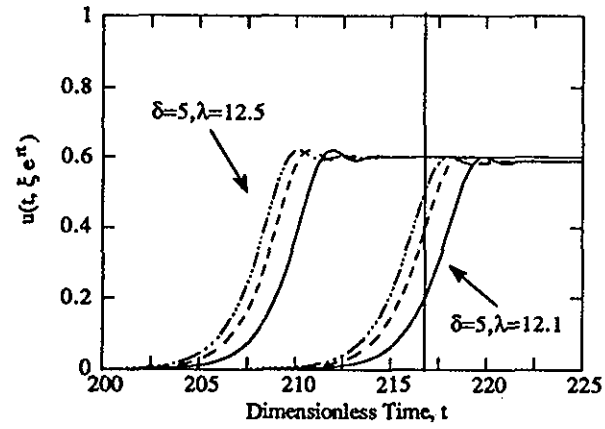

FIG. 8. Cell density evolution along three characteristics $(\xi_1,\xi_2,\xi_3) = (0.2\times10^{-70},0.5\times10^{-70},0.8\times10^{-70})$ for $r = 0.7455$, $\delta = 5$, and two λ values: 12.5 and 12.1. For the two sets, $\lambda^b = 15.661$, $\lambda^s = 12.108$. The singular solutions are $u_s = 0.6$, and $u_s = 0.586$ for the first and second sets, respectively. The vertical line denotes the time at which the characteristic ξ_3 reaches $x = 1$.

approximately equal to the expected period $T_x = T_c/(1-r) = 4.72$. The figure clearly shows the validity of Eq. (39). The initial transient clearly shows the left traveling nondispersive hyperbolic waves; after one period T_x the oscillation has advanced one wave length $L = e^{T_c} = 10.59$ in a logarithmic maturation scale, where L is given by calculating the ratio of two successive troughs in the logarithmic scale.

Below the Hopf bifurcation we expect the solutions to evolve to u_s if $\lambda > \lambda^s$, to u_{nh} if $\lambda = \lambda^s$, and to u_t if $\lambda < \lambda^s$.

Figure 8 shows the evolution of the cell density along three characteristics for $r \simeq r_{min} = 0.7455$. The results show an exponential growth, indicating that there is a maturation dependence of $u(t,x)$. The first set, for which $\lambda^b > \lambda > \lambda^s$, clearly shows that the solution converges, with damped oscillations to the singular solution u_s. For the second set ($\lambda \simeq \lambda^s$) the exponential growth, denoting spatial inhomogeneities, crosses the vertical line at $t = 216.5$, the time at which the characteristic ξ_3 reaches $x = 1$.

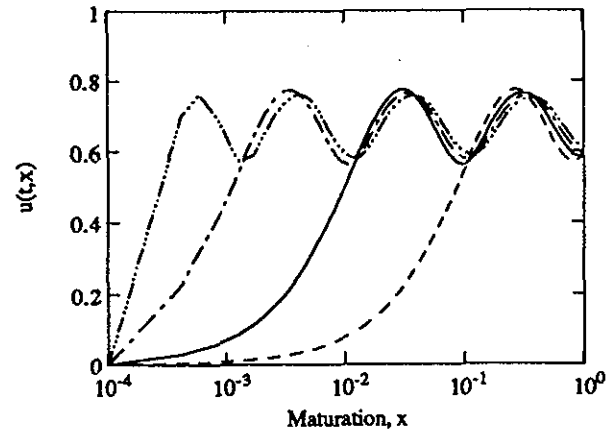

FIG. 7. Initial cell density evolution in the $(t, \ln x)$ plane for the same parameters as in Fig. 6, for $t = 4$ (dash), 8.8 (full), 13.6 (dash–dotted), 18.4 (dash–triple dotted), obtained using GFEM.

Figure 8 shows that when $P = P^s$, integration along the characteristics leads eventually to the singular solution, which is consistent with the GFEM results. It turns out that the inhomogeneous solution always approaches u_s at large x. This is explained by noting that as $t \to \infty$ and $x \to \infty$ delays play no role, and the solutions should converge to the solutions of Eq. (2) in the absence of delays. In this case, we showed in Rey and Mackey[15] that for $\lambda - \delta = r$ the solution converges to

$$u_{nh} = \frac{(\lambda-\delta)x}{(\lambda-\delta)+\lambda x}, \tag{42}$$

whose limit as $x \to \infty$ is indeed u_s.

Next we look, in more detail, at the solution behavior in the immediate vicinity of the bifurcation line $\lambda^b = \lambda^b(\delta)$.

Figure 9 shows the evolution of the cell density along three characteristics for $r \simeq r_{min} = 0.7455$ and $\lambda < \lambda^b$ (top) and $\lambda > \lambda^b$ (bottom). In both cases $\lambda^b > \lambda^s$. When λ is slightly smaller than λ^b the solution eventually converges to the singular solution through long lasting damped oscillations along the whole maturation field, analogous to a pretransitional phenomena. When λ is slightly larger than λ^b the solution oscillates without loss of amplitude around u_s, indicating the left traveling waves in the (t,x) plane.

Figure 10 shows the GFEM solution corresponding to the overdamped traveling waves for $t = 24$ (dash–dotted line) and 64 (solid line). At any fixed maturation the oscillations lose amplitude with increasing times.

5. $r_{min} < r < r_{max}$

A representative bifurcation diagram for this maturation velocity range is shown in Fig. 5. The bifurcation line crosses the stability line, but the slopes are nearly equal. Since λ^s is approximately equal to λ^b, the interaction of two important effects set in: the critical slowing down associated with the stability line $\lambda^s = \lambda^s(\delta)$ and the overdamped

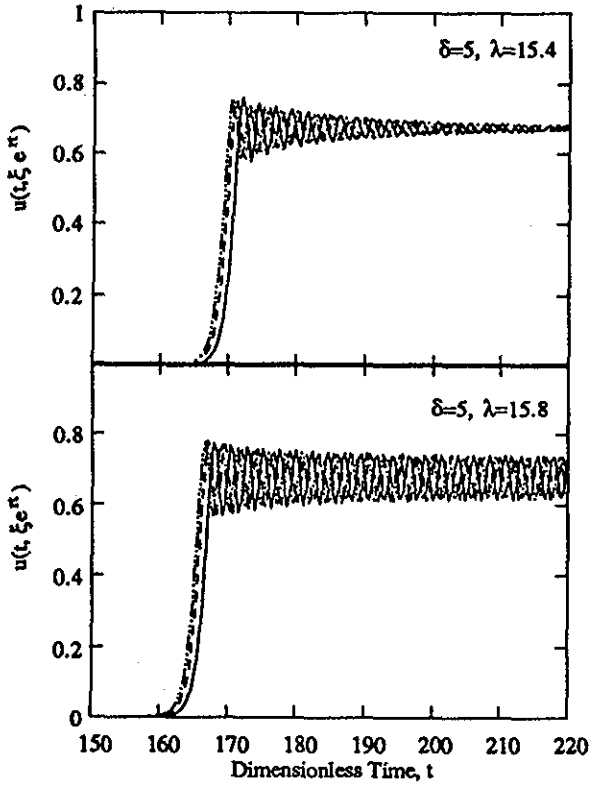

FIG. 9. Cell density evolution along three characteristics $(\xi_1,\xi_2,\xi_3) = (0.2\times10^{-70},0.5\times10^{-70},0.8\times10^{-70})$ for $r=0.7455$, $\delta=5$ and $\lambda = 15.4<\lambda^b=15.66$ (top), and $\lambda=15.8$ (bottom) $>\lambda^b=15.66$. In both cases $\lambda^b>\lambda^s=12.108$.

pretransitional oscillations associated with the bifurcation line $\lambda^b=\lambda^b(\delta)$. Furthermore, oscillations denote left traveling waves that eventually lead either to the singular solution or to the sustained oscillatory state, but they can never lead to the trivial solution. Therefore, in the range of δ for which $\lambda^s>\lambda>\lambda^b$ the solutions slowly decay without oscillations to the trivial solution, and in the range of δ for which $\lambda^s<\lambda<\lambda^b$ the solutions slowly converge through traveling overdamped waves into the singular solution. Furthermore, when λ is slightly larger than $\lambda^s>\lambda^b$ and

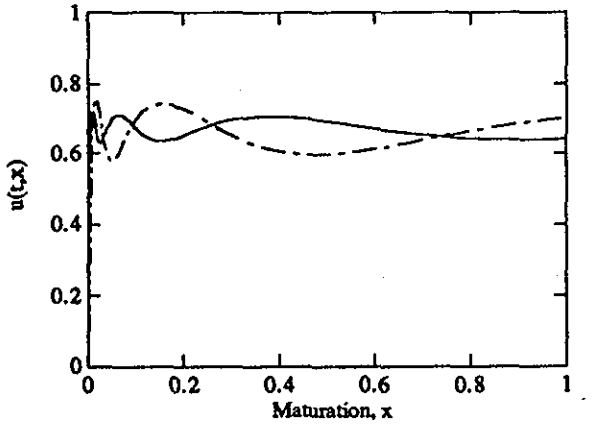

FIG. 10. Cell density profiles obtained with GFEM. $r=0.7455$, $\delta=5$, $\lambda=15.4$, $t=24$ (dash–dotted) and 64 (full).

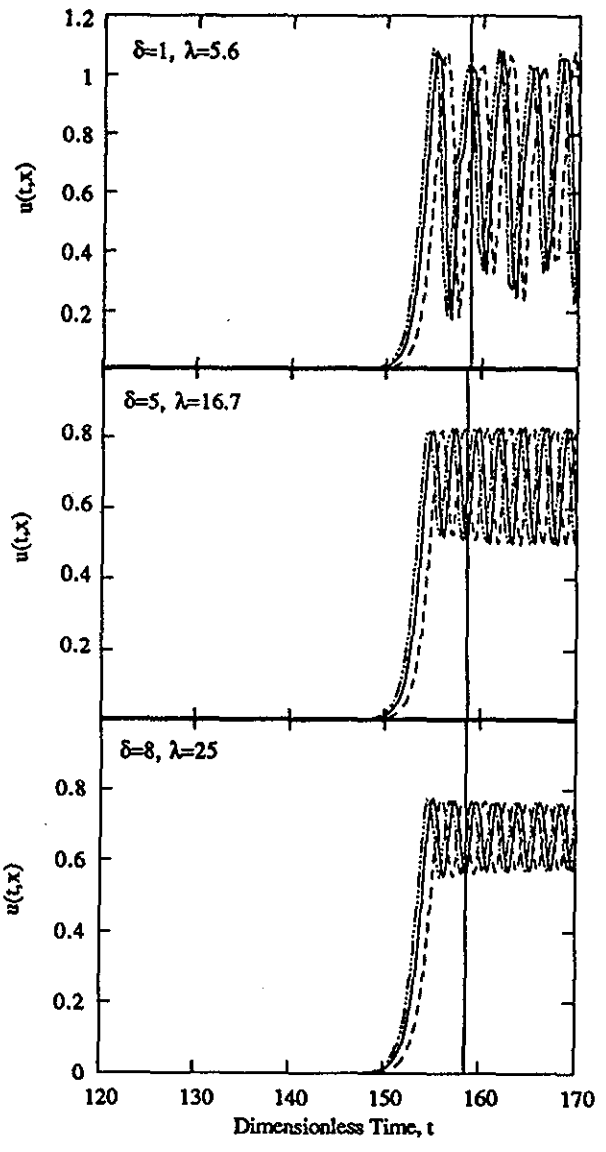

FIG. 11. Cell density evolution along three characteristics $(\xi_1,\xi_2,\xi_3) = (2\times10^{-70},5\times10^{-70},8\times10^{-70})$ for $r=1$ and three sets $(\delta,\lambda)=(1,5.6)$, (5,16.7), and (8,25). The first two sets correspond to cases where $\lambda>\lambda^s>\lambda^b$ and the third to $\lambda>\lambda^b>\lambda^s$. The vertical line has the same meaning as in Fig. 8.

when λ is slightly larger than $\lambda^b>\lambda^s$ the solutions slowly evolve into traveling waves due to the proximity to the stability line, and the dynamics is dictated by the slowly evolving boundary layer.

Figure 11 shows the evolution of the cell density along three characteristics for $r=1$, two cases corresponding to $\lambda>\lambda^s>\lambda^b$ and a third to $\lambda>\lambda^b>\lambda^s$. The first case (upper plot) exhibits oscillations not exactly around the singular solution u_s with an irregularity in the amplitude. This is attributed to the fact that the system is quenched into an unstable state. The second case (middle plot) represents a weaker quenching, since λ is now closer to λ^b. The amplitudes appear to be constant in time and the oscillations occur closer to the singular solution u_s. For the third case (lower plot) λ is slightly larger than $\lambda^b>\lambda^s$ and the oscillation is of constant amplitude and around u_s. In this range

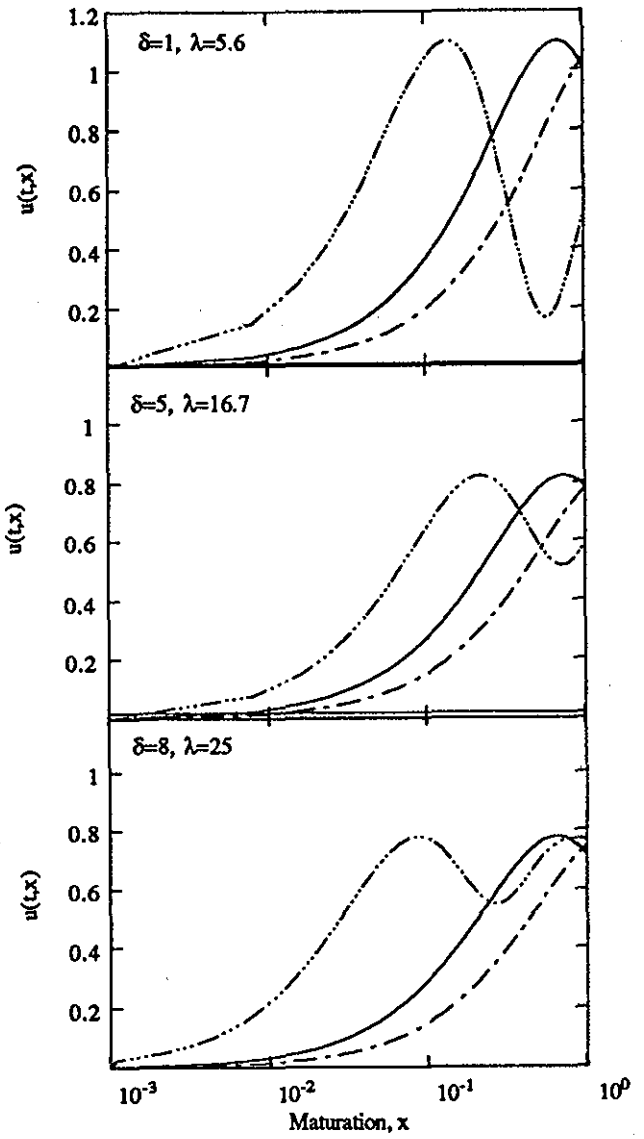

FIG. 12. Cell density profiles for the three sets of parameters as in Fig. 11, obtained with GFEM. $t = 24$ (dash–dotted), 64 (full), and 184 (dash–triple dotted). The values of u_s for the three sets are 0.82, 0.7, and 0.68.

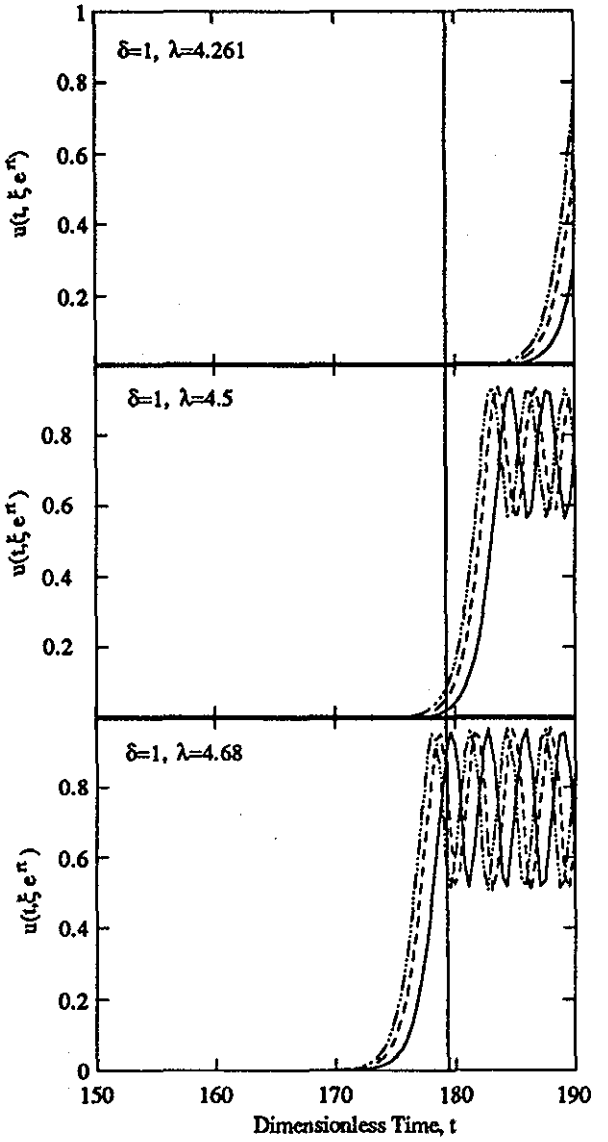

FIG. 13. Cell density evolution along three characteristics $(\xi_1,\xi_2,\xi_3) = (0.2\times10^{-70},0.5\times10^{-70},0.8\times10^{-70})$. $r = 0.9$ and $\delta = 1$, and three values λ: 4.261 (top), 4.5 (middle), and 4.68 (bottom). The vertical line denotes the time at which the characteristic ξ_3 reaches $x = 1$. For this case $\lambda^b = 4.261$ and $\lambda^s = 4.673$.

of the maturation velocity r the chosen λ values are close to λ^s and the traveling waves move with a velocity dictated by the advancing boundary layer.

Figure 12 shows the corresponding cell population profiles in a logarithmic maturation scale, obtained with GFEM. First, note that the traveling wave solutions shown in the maturation range $0 < r \leqslant r_{\min}$ should not be present here, since $T_x \to \infty$. The figures show that indeed the waves travel and that the dynamics are slow compared with previous results. There is, nevertheless, a similarity since the waves have a constant wavelength in a logarithmic maturation scale, but with a small renormalization of the expected value $L = e^{T_c}$ that decreases as we approach the intersection of the bifurcation line with the stability line. The figure also shows that as we move toward the bifurcation line there is a continuous transformation from large oscillations around lower values than u_s to smaller oscillations around u_s, and therefore these solutions are of the same type. The dynamics of the boundary layer regime is given in detail in Rey and Mackey.[15]

The solution behavior for the maturation velocity range $r_{\min} < r < r_{\max}$ in the region bounded from above by the stability line and from below by the bifurcation line is shown in Fig. 13. The upper and middle plots, for which $\lambda^s > \lambda > \lambda^b$, show that the trivial solutions are indeed stable to the traveling wave perturbations. The lower figure clearly shows the slowing down effect due to the proximity of the stability line, since even at these times the waves just start to penetrate from $x = 1$.

Finally, we examine the region bounded from above by the bifurcation line and from below by the stability line. Figure 14 shows the cell population evolution for three λ

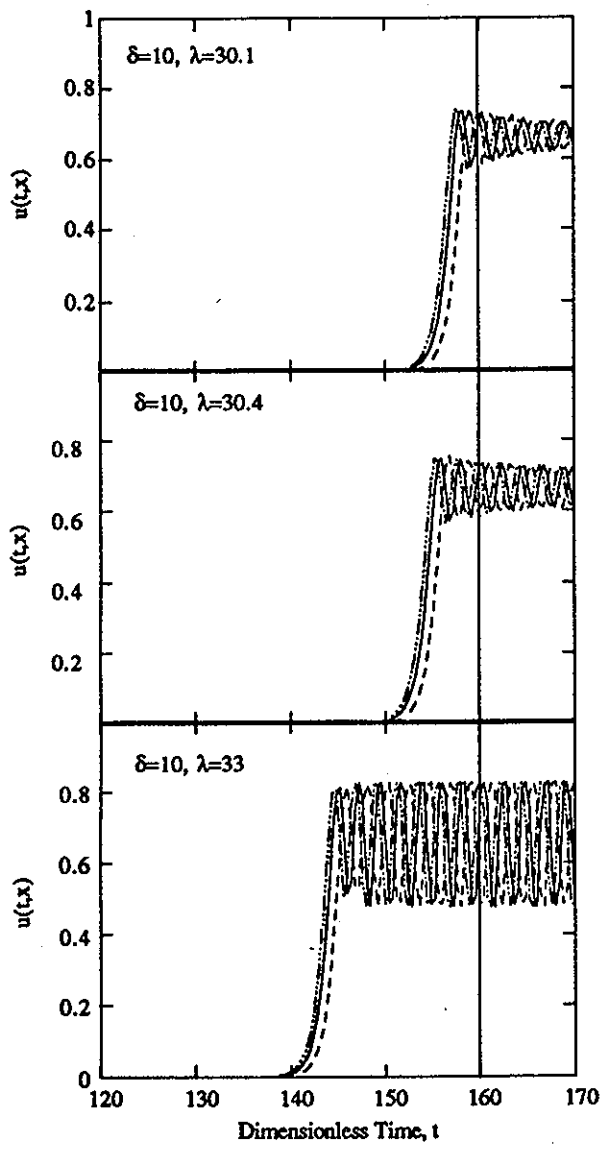

FIG. 14. Cell population evolution for $r=1$, $\delta=10$, and three λ values: 30.1 (top), 30.4 (middle), and 33 (bottom), for three characteristics $(\xi_1,\xi_2,\xi_3)=(2\times10^{-70},5\times10^{-70},8\times10^{-70})$. Again, the full line denotes the time at which the characteristic ξ_3 reaches $x=1$. For these cases $\lambda^b=30.40$.

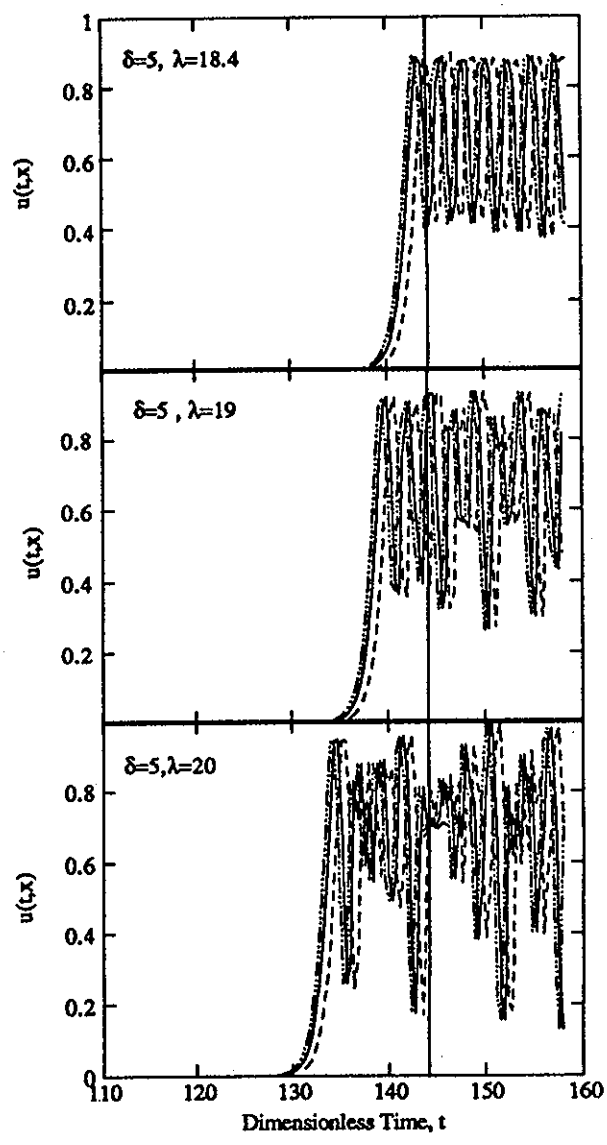

FIG. 15. Cell density evolution along three characteristics $(\xi_1,\xi_2,\xi_3)=(2\times10^{-70},5\times10^{-70},8\times10^{-70})$ for $r=1.1$, $\delta=5$, and three values of $\lambda=18.4$ (top), 19 (middle), and 20 (bottom). For the three cases $\lambda^s=18.32$ and $\lambda^b=30.40$. The vertical full line denotes the time at which the characteristic ξ_3 reaches $x=1$.

values: $\lambda<\lambda^b$ (top), $\lambda=\lambda^b$ (middle), and $\lambda>\lambda^b$ (bottom). The upper plot shows the typical overdamped oscillations with subsequent convergence to u_s. The middle plot shows the left motion of the traveling oscillations. The bottom plot shows a case corresponding to a strong quench with oscillations covering most of the maturation range. For this value of r a large value of λ does not introduce irregularities in T_c.

6. $r_{max}\leqslant r$

Now the bifurcation diagram consists of two regions defined by λ^s. For $\lambda>\lambda^s$ the solution are traveling chaotic waves u_{tcw}, when $\lambda<\lambda^s$ the stable solutions are trivial solutions u_t[13] and when $\lambda=\lambda^s$ the stable solutions are the stationary inhomogeneous solutions u_{nh}.

Figure 15 shows the evolution of the cell density ($\lambda^s=18.32$) for $\lambda>\lambda^s$. For the smallest λ the solutions oscillate with a small irregularity in the amplitude about a value lower than u_s. For a second λ the amplitude irregularities grow, and in the third case the oscillations appear to be chaotic.

Figure 16 shows the cell density profiles for four times using GFEM. From the initial linear profile the solution slowly evolves to a smooth profile with a maximum. Soon after, waves penetrate from the right with oscillations around maturation-dependent cell densities and with decreasing wavelength for increasing maturations.

Figure 17 shows the same type of behavior, but with stronger irregularities. The nature of this slow irregular oscillations is clearly distinct from the previous traveling waves, and hence we name them slow chaotic traveling

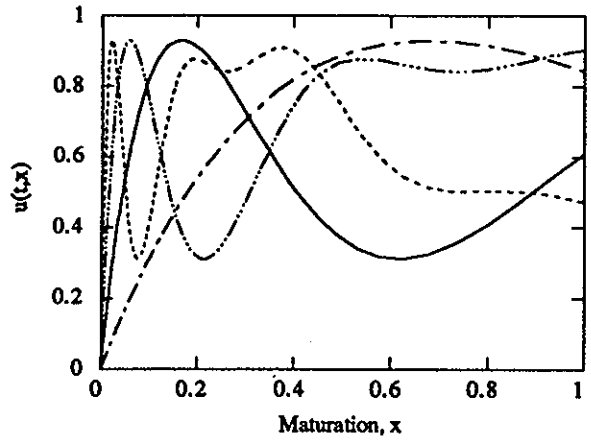

FIG. 16. Cell density profiles for $(\delta,\lambda,r) = (5,19,1.1)$ and four times $t = 40$ (dash–dashed), 88 (full), and 128 (dash–triple dotted), and 184 (dash), obtained using GFEM.

waves. These behaviors will be the object of a more extensive future study.

VI. CONCLUSIONS

The introduction of delayed arguments in a first-order partial differential equation leads to a variety of extremely rich phenomena. In this paper we have shown with a numerical example that the solutions are chaotic in a space of initial power functions; $\sigma(x) = x^p$ with p real. The possible interaction due to the proximity of attractors of a different nature gives rise to a variety of phenomena like slowing down, pretransitional phenomena, and irregular oscillations. Next, we summarize our findings for the particular initial function used in this work (also see Tables I and II).

For strictly positive initial functions, $\varphi(0) > 0$, there are three solutions: a trivial solution $u_t = 0$, a stationary spatially homogeneous solution u_{st}, and spatially homogeneous time periodic solution $u_p(t)$. The bifurcation diagram in terms of (δ,λ) consists of three regions defined by $\delta = \lambda$ and a curve $\lambda^b = \lambda(\delta)$ denoting a Hopf bifurcation.

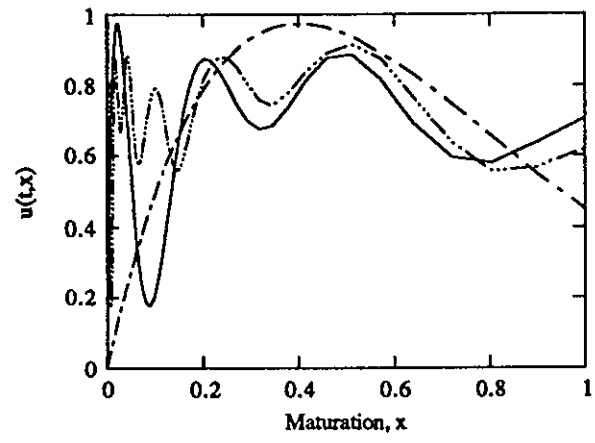

FIG. 17. Cell density profiles for $(\delta,\lambda,r) = (5,20,1.1)$ and three times $t = 24$ (dash–dashed), 64 (full), and 136 (dash–triple dotted) obtained with GFEM.

For $\lambda > \lambda^b$ the time scale t^* to reach u_p depends on r. As $r \to 0$, $t^* \to \infty$ and as $r \gg 1$, $t^* \to 0$.

When $r \leqslant r_{\min}$ the bifurcation diagram in terms of (δ,λ) consists of three regions, defined by two nonintersecting lines representing a stationary solution $[\lambda^s = \lambda(\delta)]$ and a Hopf bifurcation $[\lambda^b = \lambda(\delta)]$, and four possible solution types: a trivial solution u_t for $\lambda < \lambda^s$, a spatially inhomogeneous stationary solution $u_{nh}(x)$ for $\lambda = \lambda^s$, a spatially homogeneous singular solution u_s for $\lambda^b < \lambda < \lambda^s$, and a left traveling wave solution $u_{tw}(t,x)$ for $\lambda^b < \lambda$. The traveling waves are hyperbolic and nondispersive; the wave vector is position dependent and diverges as $x \to 0$, while the angular frequency is proportional to $(1 - r)$. The spatial and temporal oscillations are around the singular solution u_s. In a linear maturation scale the phase velocity U is a function of position: as $x \to 0$, $U \to 0$ but is constant on a logarithmic maturation scale.

When $r_{\min} < r < r_{\max}$ the lines λ^b and λ^s intersect at $\delta = \delta^*$ and the bifurcation diagram consists again of three regions and four solutions. The value of $\delta = \delta^*$ at the intersection point increases as r increases. For any given $\delta \leqslant \delta^*$ the stable solutions are u_t if $\lambda < \lambda^s$, $u_{nh}(x)$ if $\lambda = \lambda^s$, and slow left traveling waves $u_{stw}(t,x)$ if $\lambda > \lambda^s$. The slow traveling nondispersive waves $u_{stw}(x,t)$ move to the left with a phase velocity dictated by the dynamics of a boundary layer located at $x = 0$ but the wave vectors share the characteristics of the faster waves $u_{tw}(x,t)$. For any given $\delta > \delta^*$ the stable solutions are u_t if $\lambda < \lambda^s$, $u_{nh}(x)$ if $\lambda = \lambda^s$, u_s if $\lambda^s < \lambda < \lambda^b$, and $u_{stw}(t,x)$ if $\Lambda \geqslant \lambda^b$.

Finally, if $r \geqslant r_{\max}$ then $\lambda^s > \lambda^b$ for all δ, and there are two regions and three solutions: u_t if $\lambda < \lambda^s$, $u_{nh}(x)$ if $\lambda = \lambda^s$, and $u_{tcw}(t,x)$ if $\lambda \geqslant \lambda^s$, where these last solutions are slow left traveling chaotic waves describing oscillations around maturation and time-dependent cell densities.

ACKNOWLEDGMENTS

We are grateful to Professor R. Rudnicki (Katowice) for a discussion of various points in this paper, and thank the McGill University Computing Center for a grant to defray the computational costs of this research, the Natural Sciences and Engineering Research Council (Canada) for Operating Grant support to both ADR and MCM, and NATO for a Collaborative Research Grant to MCM.

[1] M. C. Mackey and J. G. Milton, Comments Theor. Biol. **1**, 299 (1990).
[2] M. C. Mackey, Blood **51**, 941 (1978).
[3] C. W. Gurney, E. L. Simmons, and E. O. Guston, Exp. Hematol. **9**, 118 (1981).
[4] C. M. Gibson, C. W. Gurney, E. O. Gaston, and E. L. Simmons, Exp. Hematol. **12**, 343 (1984).
[5] A. Lasota, Nonlin. Anal. **5**, 1181 (1981).
[6] P. Brunovský, Nonlin. Anal. **7**, 167 (1983).
[7] P. Brunovský and J. Komorník, J. Math. Anal. Appl. **104**, 235 (1984).
[8] R. Rudnicki, Ergod. Theor. Dynam. Sys. **5**, 437 (1985).
[9] R. Rudnicki, Bull. Pol. Acad. Sci. Math. **35**, 289 (1987).
[10] R. Rudnicki, J. Math. Anal. Appl. **132**, 14 (1988).
[11] K. Loskot, J. Diff. Equations **58**, 1 (1985).
[12] C. A. J. Fletcher, *Computational Galerkin Methods* (Springer-Verlag, New York, 1984).
[13] N. D. Hayes, J. London Math. Soc. **25**, 226 (1950).
[14] H. W. Stech, J. Math. Anal. Appl. **109**, 472 (1985).
[15] A. D. Rey and M. C. Mackey, Can. Appl. Math. Q. (in press).